INTECH
open science | open minds

OPEN ACCESS
ARTICLE

Nanomaterials and Nanotechnology

Preparation and Characterization of Fluorescent CdS Quantum Dots used for the Direct Detection of GST Fusion Proteins

Regular Paper

J.J. Beato-López[1], C. Fernández-Ponce[2], E. Blanco[1], C. Barrera-Solano[1], M. Ramírez-del-Solar[1], M. Domínguez[1], F. García-Cozar[2] and R. Litrán[1,*]

1 Dpto. de Física de la Materia Condensada, Universidad de Cádiz, Puerto Real(Cádiz) Spain
2 Universidad de Cadiz/ Hospital Universitario de Puerto Real, Depto. de Biomedicina, Biotecnologia y Salud Publica. Spain
* Corresponding author: rocio.litran@uca.es

Received 31 May 2012; Accepted 26 July 2012

Abstract Advances in the life sciences are now closely linked to the availability of new experimental tools that allow for the manipulation of biomolecules and the study of biological processes at the molecular level. In this context, we have optimized a synthesis process to obtain glutathione-capped fluorescent CdS nanoparticles to specifically detect Glutathione S-Transferase (GST) -tagged proteins. Using our method, based on five different heating steps, brightly fluorescent and biocompatible CdS quantum dots of different sizes can be obtained. QD optical behaviour has been evaluated studying both absorbance and fluorescence. For all the samples, the excitonic absorption onset clearly shows a blue shift at 512nm in comparison with that of bulk CdS, due to the quantum confinement effect. At increased average sizes of the nanocrystal, the emission fluorescent band shows a red shift, from 440nm to 540nm. Among different QD solutions, we demonstrate an expansion of the emission range up to ~100 nm, thus improving their features as biomarkers. Moreover we show that optimized glutathione-capped quantum dots can directly bind GST blotted onto polyvinylidene difluoride (PVDF) membranes, and thus are suitable for the direct detection of GST fusion proteins.

Keywords quantum dots, fluorescence, glutathione, glutathione S-transferase fusion protein

1. Introduction

The remarkable advances made in the fields of material science and nanotechnology over the past decade have had a significant impact on the physical, chemical and biological sciences. Specifically, current developments in the life sciences rely heavily on the availability of new experimental tools that enable the manipulation of biomolecules and the study of biological processes at the molecular and cellular levels. Progress made in the synthesis of fluorescent semiconductor nanocrystals, also known as quantum dots (QDs), together with a better understanding of their photophysical properties and the development of biocompatible surface chemistries for their solubilization, have provided new imaging probes with enormous potential for scientists in the biological sciences [1,2,3,4]. The unique optical properties of these colloidal semiconductor nanocrystals (NCs) make them

exceptional biological markers. Excitons in QDs are confined in all three dimensions, leading to a strong size dependency of optical behaviours - such as absorption – and, consequently, emission energies [5]. The radiative recombination of the charge carriers - which results in fluorescent emission when the electron falls back into the valence band - is greatly enhanced by quantum confinement, in comparison with the bulk semiconductor [6,7,8,9]. Thus, by reducing the size of certain semiconductors to a few nanometres, new fluorescent probes can be obtained. In addition, the fluorescent properties of these probes - such as their emission wavelength - can be tuned by controlling their nanometric size [1]. In comparison with organic dyes, chromophores and fluorescent proteins commonly used for fluorescent labelling, QDs have the advantage that they display size and composition-tunable emissions, narrow emission spectra and wide excitation profiles, since they are capable of being excited far beyond their emission wavelength [3,7,10,11]. This last characteristic permits the use of a single light source for the simultaneous excitation of QDs of different sizes used together as markers in multicolour applications, with the consequent decrease in costs [3,12,13,14] Moreover, QDs are very stable in relation to photobleaching and have relatively long luminescence lifetimes [1].

However, to be used in a biological environment, these nanoprobes (Nps) need to be appropriately bio-functionalized. Thus, the probe surface has to be capped with a bio-compatible and water-soluble coating. Traditionally, most methods of chemical synthesis for producing QDs have been based on the use of organic stabilizers to cap the surface atoms of Nps in order to control the growth process [15,16,17]. These methods generally use species such as trioctylphosphine oxide, long-chain amines or long-chain carboxylic acid as capping agents, which produce hydrophobic Nps and which are not compatible with the biological environment or the biomolecules to which the QDs are to be linked. In 1998, two seminal articles demonstrated that highly luminescent QDs could be made water-soluble and biocompatible by means of surface modification by the interchange of the original hydrophobic capping [2,18]. Numerous modifications of those strategies have been developed to prepare a series of group II–VI semiconductor NCs, mainly CdS, CdSe and CdTe. However, although this route provides fluorescent QDs with a large quantum yield (QY), all these methods present several disadvantages: they are expensive, environmentally-unfriendly and always require a second step for bio-functionalization. Alternatively, aqueous synthesis routes have also been developed as direct methods to obtaining biolabels [19]. Among the various stabilizers used for the preparation of QDs, natural biomolecules, such as cysteine and the tripeptide glutathione (GSH), are outstanding candidates which yield water-soluble and bio-compatible NCs. Several articles have reported the preparation of GSH-capped CdS, CdSe and CdTe Nps [17,20,21,22,23,24,25]. QDs prepared by the organic synthesis route reveal better stability and higher QY; recently, Zou et al. [24] have reported a synthesis method for obtaining highly-luminescent CdS QDs stabilized with GSH.

Based on the method of Zou et al., we have optimized a synthesis process with five different heating steps, starting at 80ºC and reaching 130ºC. By this means, we have obtained brightly-fluorescent CdS QDs of different sizes, with emission maxima ranging from 440 to 540 nm. The size dependency of the fluorescence intensity and the dynamic evolution of the fluorescence (PL) have also been evaluated. The study of the PL efficiency - as well as the PL dynamic evolution - provides information about the surface structure reconstruction of the NCs.

Interestingly, the synthesis procedure we have used does not alter the ability of the GSH moieties located on the nanoparticles to interact with the cognate ligand of GSH, Glutathione S Transferase (GST). Our data obtained with fluorescent NPs is in agreement with the data given by Chen et al. [26] and Xu et al. [27], who have reported the binding and detection of glutathione S-transferase-fusion protein by GSH-gold Nps and GSH-magnetic Nps, respectively.

Here, we show that GSH-capped CdS Nps can be used for the efficient detection of GST on the surface of PVDF membranes. Thus, GST-tagged proteins can be directly detected by this method, using the fluorescence of the nanobioconjugates.

2. Experimental details

2.1 Reagents

Cadmium chloride (99%, Sigma-Aldrich), thiourea (99%, Sigma-Aldrich) and reduced glutathione (99%, Sigma Aldrich) were used as received. All the solutions were prepared in distilled water at room temperature.

2.2 Synthesis of GSH-CdS QDs

We prepared the CdS QDs by introducing substantial changes to a previously-reported method [24]. Briefly, 0.013 mol of glutathione and 0.010 mol of $CdCl_2$ were dissolved and mixed in 150 mL of distilled water, subject to vigorous stirring. A NaOH 1M solution was added, drop by drop, until the pH of the final solution was 10. Through filtration, we removed precipitated glutathione (2.50 g) in order to avoid an excess of the capping agent in the final solution. When all the glutathione was dissolved, 0.020 mol of thiourea was slowly added. The solution - about 210 mL - was loaded in a 500 mL three–necked flask and heated in N_2 atmosphere under reflux.

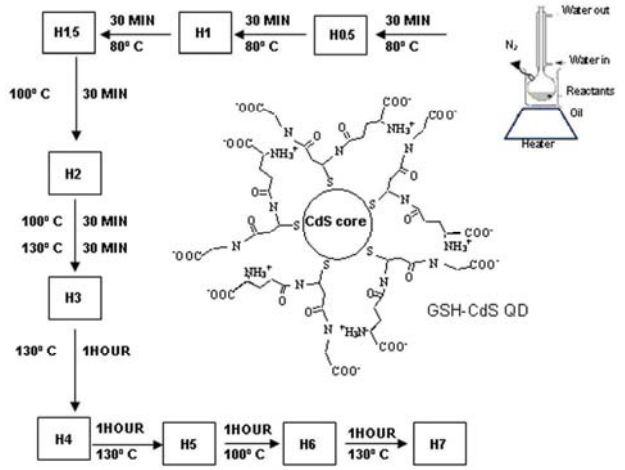

Figure 1. Experimental synthesis process to obtain the GSH capped CdS QDs.

We designed a reaction process with five different heating steps in order to obtain GSH-CdS QDs of different sizes in the same synthesis route. The final optimized procedure is summarized in Figure 1. The temperatures shown in figure 1 correspond to those measured directly in the oil bath. The corresponding temperature values in the reaction flask are: 60ºC, 75ºC and 97ºC for 80ºC, 100ºC and 130ºC, respectively.

The first heating step was performed at 80ºC for 90 minutes, and three aliquots were taken at 30, 60 and 90 minutes (samples H0.5, H1 and H1.5, respectively). A second heating step was performed at 100ºC for 1 hour, taking one aliquot at 2 hours after the start of the reaction (H2 sample). In the third step, the temperature was increased to 130ºC for 2.5 hours in order to obtain larger Nps. Aliquots were taken at 3, 4 and 5 hours from the initial time point (samples H3, H4 and H5 respectively).

The solution was cooled at 100ºC for one hour, taking an additional aliquot, corresponding to the H6 sample. Finally, in the last reaction step, we heated again at 130ºC - for one hour - obtaining the H7 sample. The reason for cooling the reaction at 100ºC for the H6 sample and then heating again to obtain H7 was to avoid the longer period at a high temperature, which could have promoted the degradation of GSH. These samples have been compared with that obtained with the shorter initial period at 80ºC (H6prev sample).

2.3 Characterization

The optical behaviour of the QDs has been evaluated studying both the absorbance and fluorescence of the Nps obtained. The absorption spectra of all the Np solutions were analysed with a "Perkin Elmer" spectrophotometer. Fluorescence emission, excitation spectra and fluorescence lifetime measurements were obtained using a "PTI Quantamaster" fluorometer. Fluorescence quantum yields (QYs) [28,29,30] were determined by comparing the integrated emission of QD solutions with that of the quinine sulphate dye with the same optical density. The excitation wavelength was set at the absorption peak of the QDs. Structural studies and average particle size estimation (measured for a number of particles exceeding 200) were obtained by TEM (Transmission electron microscopy) measurements carried out in a JEOL2011.

Lifetime measurements were made by a LaserStrobe technique using a *nitrogen/dye laser gl-3300* with a pulse width of 1 nanosecond. This technique, which is faster than TCSPC (Time-Correlation Single Photon Counting), uses a non-linear detection timescale to record the fluorescence intensity.

2.4 Glutathione S-transferase production

Glutathione S-transferase (GST) was expressed in BL21 E. coli by induction with 0.6 mM isopropyl-beta-D-thiogalactopyranoside (IPTG), followed by incubation for 4 hr at 37ºC. The harvested bacterial pellets were re-suspended with an extraction buffer (20 mM HEPES-NaOH [pH 7.5], 0.5 M NaCl, 10 mM EDTA, 0.1% Triton X-100 and 5% protease inhibitor cocktail [Sigma-Aldrich]), lysed by sonication and cleared by centrifugation. The supernatants were loaded into GSTrap FF columns (Amersham Biosciences) and the columns were washed with a washing buffer (20 mM HEPES NaOH [pH 7.5], 0.15MNaCl and 1mMEDTA) and eluted with the washing buffer containing 10 mM glutathione.

2.5 GST detection with Glutathione-NP

Volumes of 10µl and 30µl of the solution were separated in a 10% denaturing polyacrylamide gel electrophoresis (SDS-PAGE) and blotted onto PVDF membranes (BioRad™). Unspecific adsorption into the membranes was blocked in a buffer containing phosphate buffered saline (PBS) (137 mM NaCl, 2.7 mM KCl, 10 mM sodium phosphate dibasic, 2 mM potassium phosphate monobasic pH 7.4) containing 0.1% Tween and 0.5% Bovine Serum albumin (BSA), and subsequently incubated for 2 hours with a 1/10 dilution of the nanoparticle solution in PBS containing 0.1% Tween-20 and 0.5% BSA. Membranes were subsequently washed in PBS/0.1% Tween three times, 5 minutes each; then, on exposure to UV light, images were acquired by a Versadoc 5000 (BioRad™).

2.6 Cytotoxicity assay

Jurkat cells (American Type Culture Collection, Manassas, VA, USA) were maintained in Dulbecco´s Modified Eagle´s Medium (DMEM) containing 2 mM L-glutamine, 10 mM Hepes, 10% (v/v) heat-inactivated foetal bovine serum (FBS), 1% (v/v) non-essential amino

acids (NEAA), 1% (v/v) sodium pyruvate, 50 μM 2-mercaptoethanol and 100 U/ml penicillin, 100 μg/ml streptomycin at 37 ºC, 5% CO2. Quantities of $4x10^5$ cells were cultured in the absence or presence of nanoparticles in a 24 well plate. After 4 and 8 hours, cells were harvested and propidium iodide was added to stain dead cells; they were then analysed in a CyanADP-MLE™ Flow cytometer (Beckman Coulter, Inc. Fullerton, CA).

3. Results and discussion

Figure 2 shows representative TEM micrographs of H0.5, H2 and H6 GSH-QDs, as well as those corresponding to a GSH-QD solution prepared to obtain larger Nps [heating for 1 hour at 80ºC and for 5 hours at 100 ºC (H6prev sample)]. Their corresponding size distributions - obtained from TEM images - are also included in the figure. In all cases, these distributions have been fitted to a Gaussian function and the average sizes obtained from these fittings are shown in table I. All the images show homogeneous and nearly monodisperse Nps distributions, without any sign of aggregation. As expected, the average size increases for longer heating times and higher temperatures. The H6prev sample presents the highest average diameter - around 4 nm - as well as a broader size distribution, due to the shorter time of the initial reaction step at 80 ºC.

Sample	*Absorption peak (nm)*	*Brus size (nm)*	*TEM size (nm)*	*QY(%)*	*FWHM (nm)*
H0.5	320	2.31	2.43	-	119.34
H1	321	2.32	-	0.95±0.10	104.87
H1.5	322	2.33	-	2.82±0.11	104.56
H2	324	2.35	2.82	5.31±1.2	105.77
H3	364	2.74	-	26.77±1.7	106.56
H4	377	2.89	-	14.20±0.08	115.42
H5	380	2.93	-	8.61±0.07	129.34
H6	384	2.98	3.27	5.64±0.06	135.55
H7	386	3.00	-	5.25±0.07	166.54
H6-PREV	393	3.1	3.90	1.28±0.1	171.14

Table 1. Absorption band positions, TEM sizes, Brus sizes and QY percentages obtained for the different GSH-CdS QDs.

Figure 3 shows the UV-VIS-absorption spectra corresponding to all the QDs solutions obtained at different time points throughout the reaction. For all the samples, the excitonic absorption onset clearly shows a blue shift, in comparison with that of bulk CdS at 512 nm (2.42 eV). This shift of the absorption band, which corresponds to an increase in the energy gap between the valence and conduction bands of the semiconductor, provides experimental evidence for the quantum confinement in these Nps. The existence of such quantum confinement is indicative of the GSH efficiency as a capping agent for CdS cores. Thus, GSH constitutes an effective molecule for the passivation and functionalization of the QD surface, avoiding aggregation and excessive growth.

As shown in figure 1, the samples H0.5, H1 and H1.5 correspond to Nps prepared by heating at 80ºC for 30, 60 and 90 minutes respectively. These samples (figure 3) show a narrow and well-defined absorption onset at between 320 and 322 nm. When the temperature is increased to 100ºC for 30 minutes (H2 sample), the main absorption band remains in practically the same position (figure 3). Interestingly, a second less intense absorption peak was observed at 362 nm - as a shoulder relative to the first peak - at around 324 nm, indicating the start of Np growth.

When we further increase the temperature up to 130ºC, the first onset observed for the H0.5, H1, H1.5 and H2 samples disappears due to the growth of the nanocrystals while the shoulder at around 364 nm becomes the predominant absorption peak (H3 solution). For the sample H4 - treated for a longer time at 130ºC - the absorption peak shows a red shift up to 377 nm, which indicates the growth of the Nps during the reaction.

From this point on, a short shift in the absorption peak is observed as the reaction time progresses; however, a concomitant broadening of the bands takes place. The inset in figure 3 shows the biggest shift between the H2 and H3 QD solutions. The band gap for each Np solution has been calculated from the onset in the absorption spectra and the corresponding average particle size of the QDs was obtained from the correlation of each of these band gaps and particle radii using the Brus equation [5]. With this method (table 1), we obtained sizes of around 2.32 nm for samples treated at only 80ºC. The size obtained remains about 2.34 nm when we heat at 100ºC for half an hour (sample H2). The narrow absorption bands indicate the presence of a relatively small and narrow size distribution for the Nps. These results suggest that, in the first step of the reaction, small clusters of CdS (corresponding to the first onset in absorption spectra) are formed at 80ºC, which is a low enough temperature to promote the formation of a homogeneous population of small CdS nanoclusters.

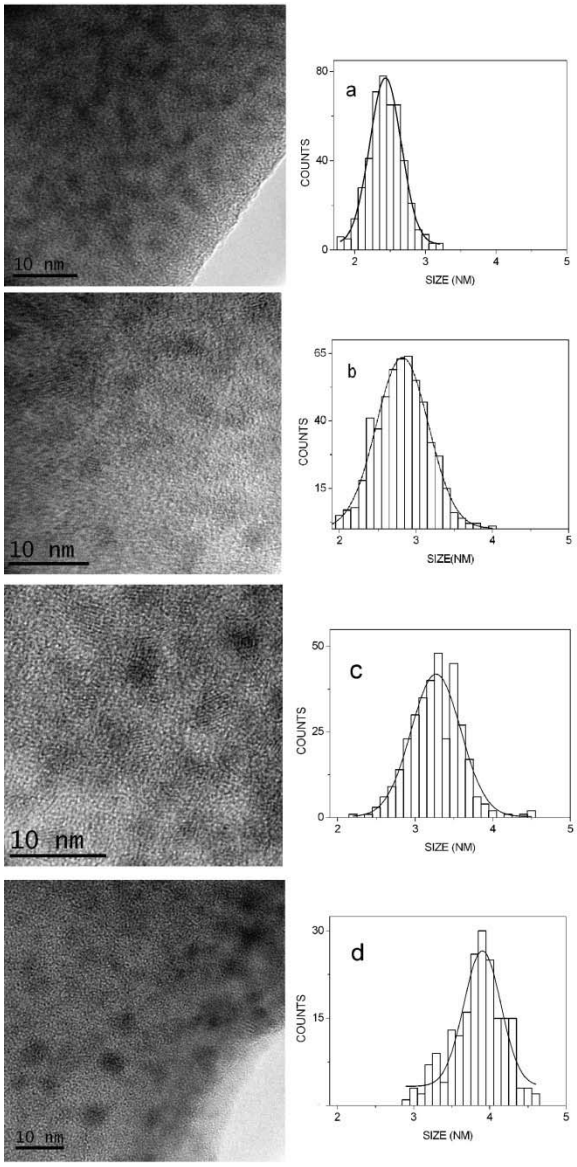

Figure 2. TEM micrographs obtained for H0.5 (a) H2 (b), H6 (c) and H6prev (d) GSH-CdS QDs solutions and their corresponding Np size distributions.

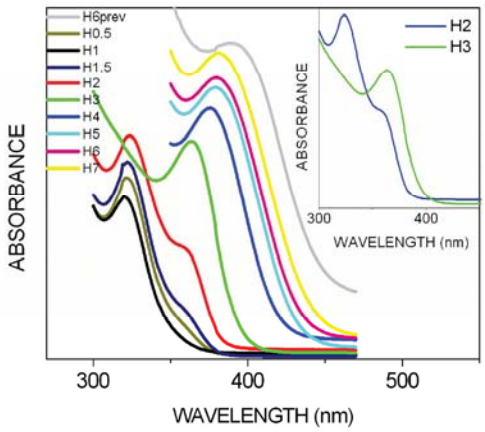

Figure 3. VIS absorption spectra corresponding to: GSH-CdS QDs obtained from the reaction flask over the course of the entire reaction process.

The results obtained for the H6prev sample, by heating for only 1 hour at 80ºC and 5 additional hours at 100ºC, show an emission band shift to red, with a maximum at 560 nm but with a broader profile, indicating greater size dispersion due to the large increase in temperature over the initial step. These results reveal that the extension of the initial heating step at low temperature (80ºC in the oil bath) makes it possible to obtain more homogeneous Nps at the smaller size range, emitting fluorescence at wavelengths lower than 500 nm.

Figure 4a shows the PL emission spectra corresponding to all the different QD solutions taken from the reaction flask at different times, using an excitation wavelength of 380 nm. All the QD solutions show a well-defined emission band with maxima located in the range between 440 and 540 nm. No evidence of broad emission bands in the 600-700 nm region - often obtained for CdS aggregates - were observed in our samples. This finding is also indicative of the formation of CdS QDs, promoted by a good passivation of those GSH molecules used as capping species.

Over the course of the entire the reaction process, as temperature and the time are increased, the PL emission peaks gradually shift to longer wavelengths due to an increase in particle size. In good agreement with the absorption behaviour, the first solutions - treated at 80ºC - show an emission band located practically at the same position, around 443 nm. Sample H3 significantly changes the position of its emission peak. For this sample, the increase in the reaction temperature clearly leads to a red shift in the emission band, centred in this case at around 481 nm. This red shift, induced by increases in the heating temperature and the reaction time, continues from H3 to H7, together with a gradual broadening in the emission bands caused by an increase in size dispersion. The QY values shown in table 1 gradually increase from the initial samples to a maximum of 26% for H3. The QY value still remains relatively high for the H4 sample and progressively decreases for larger Nps. This behaviour in the PL efficiency can be interpreted as the initial formation of those QD cores that grow with concomitant increments in PL intensity until a critical size with the highest QY is reached.

No evidence of QD fluorescence is observed for solutions treated at 130ºC for longer periods, probably due to the degradation of GSH molecules and, consequently, to the elimination of their capping effect.

We have also shown that the fluorescent behaviour of QD solutions is not dependent on the excitation wavelength. As shown in figure 4b - which depicts the fluorescent emission spectra for the H1 sample excited at different wavelengths - no major shift in the maxima position is observed as we change the excitation wavelength. This finding confirms the suitability of our Nps for multicolour applications.

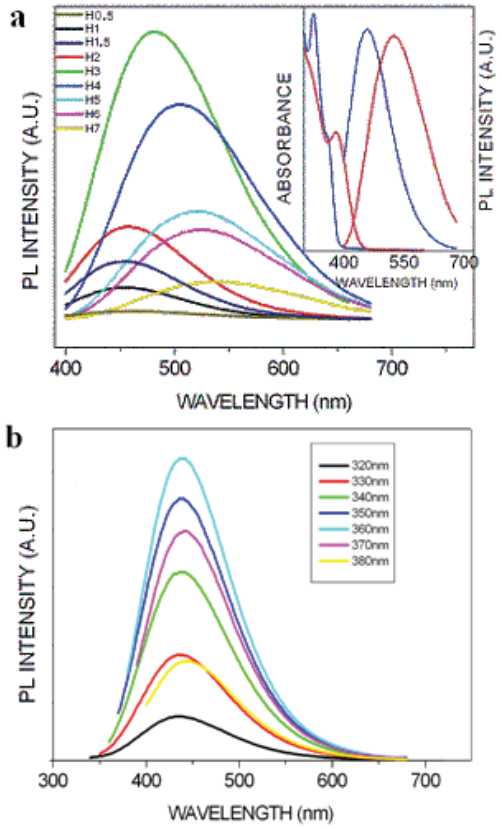

Figure 4. PL emission spectra for GSH-CdS QDs solutions obtained from the reaction flask over the course of the entire reaction process using an excitation wavelength of 380 nm (a); and PL emission spectra for the H1 sample obtained for different excitation wavelengths (b).

In summary, this synthesis procedure enables the preparation of brightly fluorescent QDs of different sizes that can be easily discriminated by the position of their fluorescence emission band. At a low temperature (80ºC), a relatively homogeneous population of small CdS cores is formed. The subsequent increase in temperature promotes the growth of these cores, which reach a critical size of about 2.74 nm by Brus approximation (H3 sample) so as to provide maximum fluorescence efficiency (QY about 26%). Regarding the method previously reported by Zou et al., we have expanded the emission range between different QD solutions by up to ~100 nm, thus improving their usefulness as biomarkers.

Additionally, the PL dynamic properties of the QD solutions have been evaluated. The PL decays obtained for all of the Np solutions fit well with a biexponential decay. For all the QD series, the PL decays clearly indicate that there are two different radiative processes responsible for the fluorescence emission. For the first decay (the faster), we obtain the values of the characteristic lifetime τ_1, ranging from 0.79 to 1.98 ns, while for the second decay (the slower) the constant time τ_2 indicates values between 11.24 and 79.69 ns. If we calculate the life-time average, $\tau_{average}$, for the whole decay process, as $\tau_{average} = B_1\tau_1^2 + B_2\tau_2^2 \ / \left(B_1\tau_1 + B_2\tau_2\right)$, where B_1 and B_2 are the pre-exponential factors for the fast and slow processes respectively, we find that the H3 sample shows the maximum value.

Different possible explanations for such multi-exponential decay have been proposed [9,11,31]. In accordance with the explanation proposed by Zhang [31] et al., we suggest that more than one radiative recombination channel of excitons exists. The fast PL decay component may originate from the recombination of the de-localized carriers in the internal states, whereas the slow PL decay can be attributed to the recombination of the localized carriers at the surface, where both radiative and non-radiative traps are located.

Figure 5 shows both the PL QY percentage as well as the PL $\tau_{average}$ versus Nps Brus diameter. A similar tendency is observed for the two parameters. For the smallest Nps, the PL QY initially increases with the Np size, due to the decrease in the surface-to-volume ratio and, consequently, to the lower proportion of surface disorder and surface degradation, provoking non-radiative surface transitions via the surface traps.

However, this tendency is not observed in all the diameter range: the QY reaches a maximum value of around 2.7 nm (H3 sample), after which the PL QY starts to decrease as the Np size increases. This evolution can be explained on the basis of the competition between two phenomena: the already mentioned surface-to-volume ratio and the lattice contraction due to the surface tension in Nps with a lower diameter. This surface tension is considerably stronger for smaller Nps, provoking a process of reconstruction of the surface and thus minimizing the number of non-radiative surface traps; hence, their negative contribution to PL QY. This contraction in the lattice constant has been confirmed by HRTEM images, from which we have measured the lattice parameter for different samples and obtained a reduction of 6% for the smaller sizes. However, for the extremely small Nps (diameters of less than 2.3 nm), the high surface-to-volume ratio leads to an excessive number of non-radiative traps per unit volume (despite an improvement of surface quality).

Attending to the $\tau_{average}$ evolution, we find that, for the smaller Nps, the initial absolute increment of the surface value contributes to the increase in total lifetime - mainly affected by the slow component at the Np surface. As the QD size increases and, consequently, the surface per unit volume decreases, a slow decrease in the $\tau_{average}$ parameter is observed.

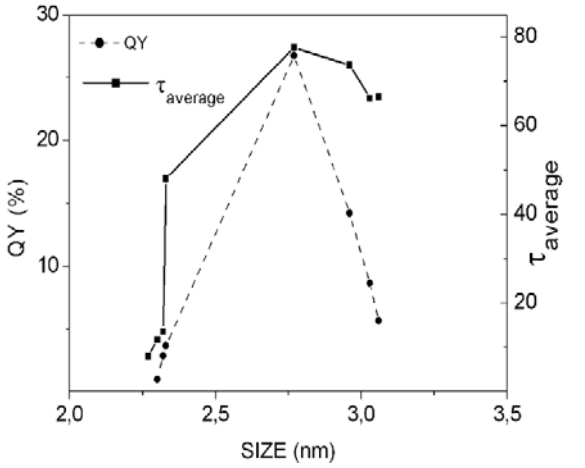

Figure 5. Size dependence of the PL QY and $\tau_{average}$ fluorescence lifetime

In order to evaluate the influence of Np size on fluorescence efficiency, we have to consider two phenomena competing in opposing directions: surface reconstruction due to lattice contraction and surface/volume ratio. In general, we have small Nps (Brus diameters of less than 4 nm). For these sizes, the lattice contraction effect should contribute to optimizing the Np surface, increasing the QY and the average time effects for smaller Nps. Considering the effect of the lattice contraction only, the QY and average time should decrease when the size increases. This is the behaviour observed for diameters of between 2.7 and 3.2 nm. However, for the smallest Nps (diameters of less than 2.7 nm) the large surface/volume ratio enhances the effect of surface traps, leading to a decrease in the efficiency of the fluorescence process. For this regime (extremely small Nps), the surface/volume effect is more significant than the lattice contraction and the number of traps that appear is greater than the number that are repaired.

We have used the most fluorescent QD solution (H3 sample) in the experiments for the detection of GST fusion proteins. Given the harsh process that binding to a NP implies for a biomolecule such as glutathione, we were interested in ascertaining whether binding to its cognate molecule GST was preserved. Thus, we performed experiments in order to detect a GST protein after separation, by means of a SDS-PAGE and subsequent blotting onto a PVDF membrane. Recombinant GST was expressed in E-coli bacteria and resuspended on denaturation buffer containing SDS and 2-Mercaptoethanol. Proteins present in the bacterial lysates were separated, depending upon their molecular weight. As shown in Figure 6, GST is detected as a single fluorescent band on the incubation of the membrane with Glutathione-QD. Our results imply not only that the GST protein has been renatured onto the membrane (since it has been shown, broadly, that the renaturation step is pivotal for the far western technique [32]) but also that the Glutathione has retained its ability to bind GST regardless of the harsh treatment it has endured.

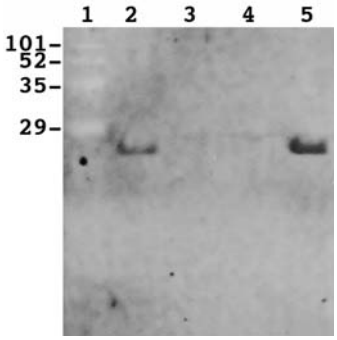

Figure 6. SDS-PAGE image of the protein glutathione S transferase expressed in E. Coli as recognized by GSH-CdS QDs. Lane 1: molecular markers with a molecular weight in kDa shown to the left. Lane 2 and lane 5: 10 and 30 μl of bacterial lysate respectively.

To ascertain the biocompatibility of the QD solutions, we added nanoparticles to cell cultures and analysed cell death at 4 (data not shown) and 8 hours. As shown in figure 7, the percentage of dead cells (stained with Propidium Iodide) is similar to that in the control cultures in the absence of nanoparticles. Interestingly, fluorescence can be observed in the channel corresponding to NP emission (2.25% in H4 or 2.14% in H6 compared to 1.17% in the control), indicating that some nanoparticles adhere to the cells. It is also of interest that there is no increase in cell death, even in this nanoparticle-stained population.

4. Conclusions

We have optimized a synthesis procedure for producing different sizes of GSH-capped water-soluble CdS QDs emitting fluorescence with a relatively large QY. The difference in QD diameters is enough to generate Nps with fluorescent peaks located in a range of ~100 nm. The emission bands are narrow and the positions of the peaks are independent of the excitation wavelength for a wide range, which makes them suitable candidates for biological fluorescent probes in multicolour experiments.

The Nps obtained show homogeneity and a monodispersion of size, together with a concomitant increase in the Np diameter as the reaction temperature and heating time are increased. The competition between the two factors - the surface-to-volume ratio and the surface reconstruction due to the surface tension in small Nps - leads to the existence of a critical Np diameter with an optimal surface/reconstruction, for which the non-radiative processes contributing to the decrease of PL QY reach a minimum.

We have demonstrated that the GSH-capped CdS QDs can directly bind GST protein blotted onto PVDF membranes, proving the suitability of our bioconjugated QDs for the direct detection of GST fusion proteins.

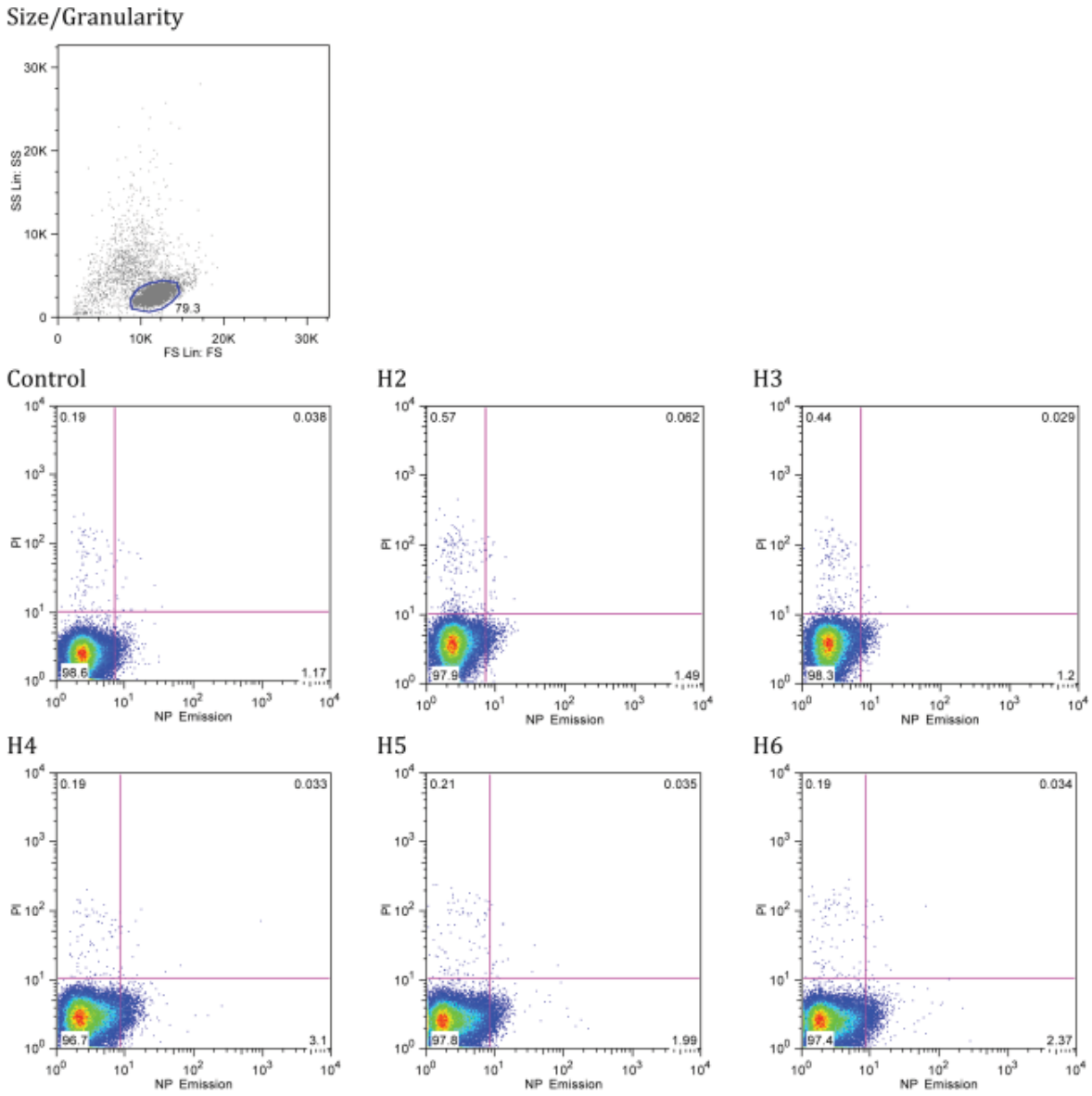

Figure 7. Flow cytometry colour plot of Jurkat cells incubated with the corresponding NPs. The Jurkat cells were electronically gated according to size/granularity distribution (upper plot). Propidium Iodine (PI) stained cells (dead cells) vs. NP stained cells (NP emission using a 450/50 or a 530/40 optical filter for H2-H3 and H4-H6 respectively) for gated cells are shown in the remaining 6 panels. The percentage of cells in each quadrant is shown.

5. Acknowledgments

The authors acknowledge the financial support of the Innovation and Science Ministry (PN/PETRI/PR/2007-019) and the Junta de Andalucia (P08-CTS-04348).

6. References

[1] A. P. Alivisatos, "Semiconductor clusters, nanocrystals and quantum dots", *Science*, vol. 271, pp. 933-993, 1996.

[2] M. Bruchez, M. Moronne, P. Gin, S. Weiss, A. P. Alivisatos, "Semiconductor Nanocrystals as fluorescent biological labels", *Science*, vol. 281, pp. 2013-2016, 1998.

[3] D. R. Larson, W. R. Zipfel, R. M. Williams, S. W. Clark, M. P. Bruchez, F. W. Wise, W. W. Webb, "Water-Soluble Quantum Dots for Multiphoton Fluorescence Imaging in Vivo", *Science*, vol. 300, pp. 1434-1436, 2003.

[4] X. Michalet, F. F. Pinaud, L. A. Bemtolilla, J. M. Tsay, S. Doose, J. J. Li, G. Sundaresan, A. M. Wu, S. S. Gambhir, S. Weiss, "Quantum Dots for Live Cells, in Vivo Imaging, and Diagnostics", *Science*, vol. 307, pp. 538-544, 2005.

[5] L. E. Brus, "Electron-electron and electron-hole interactions in small semiconductor crystallites: The size dependence of the lowest excited electronic state", *J. Chem. Phys*., vol. 79, pp. 5566-5571, 1983.

[6] B. Dubertret, P. Skourides, D. J. Norris, V. Noireaux, A. H. Brivanlou, A. Libchaber, "In vivo imaging of quantum dots encapsulated in phospholipid miscelles", *Science*, vol. 298, pp. 1759-1762, 2002.

[7] J. E. Bowen Katari, V. L. Colvin, A. P. Alivisatos, "X-ray Photoelectron Spectroscopy of CdSe Nanocrystals with Applications to Studies of the Nanocrystal Surface", *J. Phys. Chem*., vol. 98, pp. 4109-4117, 1994.

[8] M. G. Bawendi, P. J. Carroll, W. L. Wilson, L. E. Brus, "Luminescence properties of cadmium selenide quantum crystallites: resonance between interior and surface localized states", *J. Chem. Phys*, vol. 92, pp. 946-954, 1992.

[9] W. Z. Lee, G. W. Shu, J. S. Wang, J. L. Shen, C. A. Lin, W. H. Chang, R. C. Ruaan, W. C. Chou, C. H. Lu, Y. C. Lee, "Recombination dynamics of luminescence in colloidal CdSe/ZnS quantum dots", *Nanotechnology*, vol. 16, pp. 1517-1521, 2005.

[10] V. L. Colvin, M. C. Schlam, A. P. Alivisatos, "Light-emitting diodes made from cadmium selenide nanocrystals and a semiconducting polymer", *Nature*, vol. 370, pp. 354-357, 1994.

[11] D. Valerini, A. Cretí, M. Lomascolo, L. Manna, R. Cingolani, M. Anni, "Temperature dependence of the photoluminescence properties of colloidal CdSe/ZnS core/shell quantum dots embedded in a polystyrene matrix", *Phys. Rev.* B, vol. 71, id. 235409, 2005.

[12] X. Gao, W. C. W. Chan, S. Nie, "Quantum dots nanocrystals for ultrasensitive biological labeling and multicolor optical encoding", *Journal of Biomedical Optics*, vol. 7, pp. 532-537, 2002.

[13] J. M. de la Fuente, S. Penedés, "Glyco-quantum dots: a new luminescent system with multivalent carbohydrate display", *Tetrahedron: Asymmetry*, vol. 16, pp. 387-391, 2005.

[14] M. N. Rhyner, A. M. Smith, X. Gao, H. Mao, L. Yang, S. Nie, "Quantum dots and multifunctional nanoparticles: new contrast agent for tumor imaging", *Nanomedicine*, vol. 1(2), pp. 1-9, 2006.

[15] C. B. Murray, D. J. Norris, M. G. Bawendi, "Synthesis and characterization of nearly monodisperse CdE (E = sulfur, selenium, tellurium) semiconductor nanocrystallites", *J. Am. Chem. Soc*., vol. 115, pp. 8706-8715, 1993.

[16] N. Tessler, M. Medvedev, M. Kazes, "Efficient Near-Infrared Polymer Nanocrystal Light-Emitting Diodes", *Science*, vol. 295, pp. 1506-1508, 2002.

[17] C. Barglik-Chory, D. Buchold, M. Schmitt, W. Kiefer, C. Heske, C. Kumpf, O. Fuchs, L. Weinhardt, A. Stahl, E. Umbach, M. Lentze, j. Geurts, G. Muller, "Synthesis, structure and spectroscopic characterization of water-soluble CdS nanoparticles", *Chem. Phys. Lett.*,vol. 379, pp. 443-451, 2003.

[18] W.C.W. Chan, S. Nie, "Quantum Dot Bioconjugates for Ultrasensitive Nonisotopic Detection", *Science,* vol. 281, pp. 2016-2018, 1998.

[19] L. Spanhel, M. Haase, H. Weller, A. Henglein, "Photochemistry of colloidal semiconductors. 20. Surface modification and stability of strong luminescing CdS particles", *J. Am. Chem. Soc*., vol. 109, pp. 5649-5655, 1987.

[20] Y. F. Chen, Z. Rosenzweig, "Luminescent CdS Quantum Dots as Selective Ion Probes", *Anl. Chem*., vol. 74, pp. 5132-5138, 2002.

[21] Y. Zheng, S. Gao, J. Y. Ying, "Synthesis and Cell-Imaging Applications of Glutathione-Capped CdTe Quantum Dots", *Adv. Mater*., vol. 19, pp. 376-380, 2007.

[22] A. P. Alivisatos, "The use of nanocrystals in biological detection", *Nat. Biotechnol*., vol. 22, pp. 47-52, 2004.

[23] C. Jiang, S. Xu, D. Yang, F. Zhang, W. Wang, "Synthesis of glutathione-capped CdS quantum dots and preliminary studies on protein detection and cell fluorescence image", *Luminescence*, vol. 22, pp. 430-437, 2007.

[24] L. Zou, Z. Fang, Z. Gu, X. Zhong, "Aqueous phase synthesis of biostabilizer capped CdS nanocrystals with bright emission", *Journal of Luminescence*, vol. 129, pp. 536-540, 2009.

[25] M. Xue, X. Wang, H. Wang, B. Tang, "The preparation of glutathione-capped CdTe quantum dots and their use in imaging of cells", *Talanta*, vol. 83, pp. 1680-1686, 2011.

[26] C. T. Chen, W. J. Chen, C. Z. Liu, L. Y. Chang, Y. C. Chen, "Glutathione-bound gold nanoclusters for selective-binding and detection of glutathione S-transferase-fusion proteins from cell lysates", *Chem. Comm*., pp. 7515-7517, 2009.

[27] Y. Pan, M. J. C. Long, X. Li, J. Shi, L. Hedstrom, B. Xu, "Glutathione (GSH)-decorated magnetic nanoparticles for binding glutathione-S-transferase (GST) fusion protein and manipulating live cells", *Chem. Sci*., vol. 2, pp. 945-948, 2011.

[28] M. Baumble, D. Stamou, J. M. Segura, R. Hovius, H. Vogel, "Highly Fluorescent Streptavidin-Coated CdSe Nanoparticles: Preparation in Water, Characterization, and Micropatterning", *Langmuir*, vol. 20, pp. 3828-3831, 2004.

[29] D. F. Eaton, "Reference materials for fluorescence measurement", *Pure & Appl. Chem*., vol. 607, pp. 1107-1114, 1988.

[30] J. N. Demas, G. A. Crosby, "Measurement of photoluminescence quantum yields", *J. Phys. Chem*, vol. 75(8), pp. 991-1024, 1971.

[31] J. Zhang, X. Zhang, J. Y. Zhang, "Size-Dependent Time-Resolved Photoluminescence of Colloidal CdSe Nanocrystals" *J. Phys. Chem.* C, vol. 113, pp. 9512-9515, 2009.

[32] D. G. Edmondson, S. Y. R. Dent, "Identification of protein interactions by far western analysis", *Current Protocols in Protein Science*, 2001, pp. 19.7.